Identification of Fibrillatory Sources by Measuring Causal Relationships

Miguel Rodrigo[1], Maria S Guillem[1], Alejandro Liberos[1], José Millet[1], Omer Berenfeld[2], Andreu M Climent[1]

[1]Bio-ITACA, Universitat Politecnica de Valencia, Valencia, Spain
[2]Center for Arrhythmia Research, University of Michigan, Ann Arbor, USA

Abstract

Atrial fibrillation (AF) is a complex arrhythmia whose mechanisms of onset, maintenance and termination are not yet understood. Recent studies have demonstrated that the isolation of specific regions of the atria can terminate the arrhythmia. These results suggest a hierarchical organization where certain parts of the atria are determining the electrical activity of the whole tissue, acting as electrical sources. In this work, we present and validate a methodology able to identify atrial sources during AF by using causal relationships. The performance of the presented technique has been illustrated by using mathematical models and real signals obtained with optical mapping under different fibrillatory scenarios.

1. Introduction

Atrial Fibrillation (AF) is a complex and self-sustained arrhythmia which affects about 4% of the total population. This fibrillatory process is characterized by an irregular propagation of the electrical signal across the atria making the myocardium completely inefficient in their mechanical functions. Some authors have postulated that cardiac fibrillation is caused by a set of randomly generated waves which crosses the myocardium colliding with each other and forming new waves [1]. However, several authors defend the theory that fibrillatory processes are governed by a hierarchical pattern, where specific areas of the myocardium are responsible of the onset and/or maintenance of the arrhythmia [2]. During the last years, computer modeling together with the use of voltage-sensitive probes and high-resolution video imaging to record electrical wave propagation on the surface of isolated hearts has led to a better characterization of the dynamics of AF and of its nature. Those analyses have enforced the rotor theory as an important mechanistic explanation for AF [3]. However, the postulation that a single rotation circuit may be capable of generating and maintaining fibrillatory activity indefinitely remains in the focus of debate. In this work, we will make use of mathematical models and optical mapping recordings to evaluate the potential use of causal relationships to identify the existence of a cardiac region which governs the electrical propagation in the entire myocardium. Together with the clarification of AF mechanisms, the presented methodology may be useful for clinical identification of ablation targets.

2. Database

2.1. Mathematical models

A 2-D model of human myocardial tissue including current dynamics in the atria was used to obtain mathematical simulations [4]. Euler integration method was applied to solve the differential equations with a time resolution of 0.005 ms. Three different scenarios were simulated: (1) a uniform sphere (2 cm radius) with a focal propagation pattern (Fig. 1.1A); (2) a sphere (2 cm radius) where 20% of its surface had physiological parameters of the left atrium (LA), and the remaining 80% of the surface had the physiological properties of the right atrium (RA) [4] and in which two stable rotors maintain the fibrillation (Fig. 1.2A); and (3) a plane (3x3 cm) with 20% of LA tissue in the center surrounded by RA. In this case the propagation pattern was originated by one stable rotor in the center of the LA and fibrillatory conduction in the RA (Fig. 1.3A).

From each mathematical simulation, a uniform mesh of pseudo-unipolar electrograms was calculated under the assumption of a homogenous, unbounded and quasi-static medium by using the following expression:

$$V_{\vec{r}} = \sum_{\vec{r}} \left(\frac{\vec{r}}{r^3}\right) \cdot \vec{\nabla} V_m \qquad (1)$$

where $\vec{r}$ is the distance vector between the measuring point and a point in the tissue domain (r is the distance scalar), and $\vec{\nabla}$ denotes the gradient operator. Computed electrograms were stored for its latter processing at a sampling frequency of 1 kHz.

2.2. Optical mapping recordings

The optical data was obtained from an isolated Langerdoff-perfused sheep heart. Two 14-bit-CCD cameras were directed toward a 2x2 cm area of the left atrial appendage (LAA) and the posterior left atrium (PLA) and 2 optical fibers connected to a laser served as illumination at 532 nm. Several movies were recorded at a sampling frequency of 400 Hz, with a resolution of 80x80 pixels. These movies were background subtracted and spatio-temporally filtered using averaging with temporal and spatial windows of 3 ms and 5 pixels. Three movies were chosen to validate the proposed methodology: one during pacing, i.e. focal propagation (Fig. 2.1A); one from the LAA with an 8-figure rotatory pattern (Fig. 2.2A); and one from the PLA with a rotatory pattern and fibrillatory conduction (Fig. 2.3A).

3. Methods

Causal relations were searched between *N* neighboring signals placed on a uniform mesh. Signals were divided into K_n 50% overlapping segments of length equal to the inverse of the dominant frequency. The autoregressive model (ARM) and measurement of influence were used to assess causal relationships between signal sections of neighboring nodes. Results were summarized into a recurrence map (RM).

3.1. Autoregressive modeling

Each pair of simultaneous observations $x_i(t)$ and $x_j(t)$ obtained from neighboring nodes, was assumed to be represented by an:

$$x_i(t) = \sum_{\tau=t_{min}}^{t_{max}} a_\tau \cdot x_j(t-\tau) + \varepsilon_{ij}(t) \quad (1)$$

where a_τ were the ARM coefficients, and $\varepsilon_{ij}(t)$ was the error in the prediction of x_i from x_j, which can be assumed to be a white noise process characterized by its variance $\sigma^2_{\varepsilon_{ij}}$. The order of the ARM model was given by the size of the search window t_{max}-t_{min}. ARM coefficients were estimated by using the least-squares method.

3.2. Causal relations

Since large variances in the prediction error $\sigma^2_{\varepsilon_{ij}}$ can be attributed to a weak dependency between source and destiny signals, the $\sigma^2_{\varepsilon_{ij}}$ was used to assess the degree of causality between two signals. However, in order to compare on equal terms the degree of causality between different signals with inherent differences in their variance, we used a statistical approach based on influence measure. This measure compares the variance value obtained by applying the ARM model in the source signal $\sigma^2_{\varepsilon_{ij}}$ with the variance value $\sigma^2_{\varepsilon_{ii}}$ obtained by applying the model on the signal itself. We defined the Influence Ratio matrix (IR), computed for a given pair if signals (i,j) as the ratio between variances of the error of ARM models for the source signal ($\sigma^2_{\varepsilon_{ij}}$) and for itself ($\sigma^2_{\varepsilon_{ii}}$):

$$\mathrm{IR}_{ij} = \frac{\sigma^2_{\varepsilon_{ii}}}{\sigma^2_{\varepsilon_{ij}}} \quad (2)$$

In order to evaluate causal relationships of an entire recording, the signal was divided in K_n overlapping time intervals and the IR was measured for each interval ($\mathrm{IR}_{\mathrm{ij,k}}$). Finally, the influence of a signal x_j in a signal x_i was summarized by normalizing the IR matrix:

$$\mathrm{IRN}_{ij} = \frac{\frac{1}{K_n}\sum_{k=1}^{K_n} IR_{ij,k}}{\frac{1}{K_n}\sum_{k=1}^{K_n}\sum_{i=1}^{N} IR_{ij,k}} \quad (3)$$

Notice that by normalizing all IRNs we are setting $\sum_{i=1}^{N} \mathrm{IRN}_{ij} = 1$, which means that the activity of each electrode is assumed to be the result of the combination of all other signals.

Once the influence of each node in all the other nodes was measured, a Recurrence Map (RM) was constructed by assigning a value between 0 and 1 to each node according to the probability that the signal comes from that node (i.e. 1 in for source points, 0 for sink points). These probability values (P) were computed by using the following expression:

$$P = M^{\infty} \times P_0; \quad (4)$$

where M^{∞} was the permanent regime value of IRN matrix and P_0 was the initial probability distribution where $P_{0i} = 1/N$. M^{∞} was iteratively computed as follows:

$$\mathrm{M}^t = \mathrm{M}^{t-1} \times \mathrm{M}^{t-1}, \quad \mathrm{M}^0 = \mathrm{IRN} \quad (5)$$

$$\xi = \max(\mathrm{M}^t - \mathrm{M}^{t\text{-}1}) \quad (6)$$

M^{∞} was reached when ξ was below a threshold.

3.3. Estimation of conduction velocity

The presented method estimated causal relations of neighboring electrodes within a given search window. The rationale under this assumption was that causal relations that imply propagation velocities above or below a physiological range should be disregarded. Causal relation maps computed for non-physiological search windows may result in unstable measurements and thus the search window that results in higher temporal stability should be selected. This temporal stability was estimated by measuring an organization index (OI) for each IR value:

$$OI_i = \left| \frac{1}{K_n} \sum_{k=1}^{K_n} \frac{\sum_{j=1}^{J_n} IR_{ij,k} \cdot \vec{u}_{ij}}{\left| \sum_{j=1}^{J_n} IR_{ij,k} \cdot \vec{u}_{ij} \right|} \right| \quad (7)$$

where $\vec{u}_{ij}$ is the unit vector connecting nodes i and j and OI_i depends on the t_{max} and t_{min} values chosen for computing IR indexes. Temporal stability (TS) in causal relation estimation was measured as follows:

$$TS = \frac{1}{N} \sum_{i=1}^{N} OI_i \cdot \frac{N}{\sum_{i=1}^{N} \sigma_{OI_i}^2} \quad (8)$$

where $\sigma_{OI_i}^2$ was the variance of OI values in the neighbourhood of i. Finally, t_{max} and t_{min} values that maximize TS were chosen.

4. Results

4.1. Mathematical models

Fig. 1.1A shows an example with a uniform tissue under organized propagation originated from a stable point. In this case, the electrical activity of the whole atrium was leaded by this point. The RM shown in Fig. 1.1B has only one region with high values (i.e. 0.38), matching with the focal area.

The second simulation had two stable rotors: one rotor located in the center of the LA region and another rotor in the RA, close to the RA/LA frontier (Fig. 1.2A). This two rotors governed the activity of the whole tissue, i.e., any activation anywhere in the tissue was caused by a propagation from one of these two rotors. Each rotor leads the activity of the atrium in which it was located, and thus both rotors had the similar hierarchical relevance. The RM (Fig. 1.2B) showed high values in the position of the two rotors (i.e. 0.096 and 0.075 for the rotor in the LA and RA respectively). Other regions of the tissue presented values closer to zero.

The third mathematical simulation presented a stationary rotatory pattern in the LA tissue which was situated in the center of the simulated area, and an irregular fibrillatory propagation to the rest of the tissue (Fig. 1.3A). Although LA rotor governed the electrical activity to the whole tissue, fibrillatory conduction provided secondary rotors that were created and destroyed during the simulation time. Some of those rotors generate were temporally stable and form eight-figure rotors. One example appeared in the upper left corner during almost the entire simulation. According to the described propagation pattern, the RM (Fig. 1.3B) showed highest values in the position of the main rotor (i.e. 0.051). In other regions of the tissue, values closer to zero were measured. Notice that secondary rotors presented intermediate values (i.e. 0.008) indicating that the closest region around those rotations were at least partially caused by its activity.

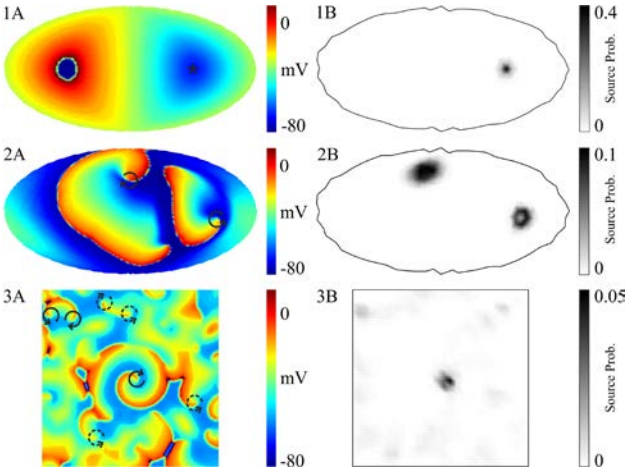

Figure 1. Transmembrane potential (A) and Recurrence Map (B) from mathematical models: (1) a focal propagation, (2) a propagation pattern governed by two rotors, (3) a propagation pattern governed by a stable rotor in the center and fibrillation conduction in the periphery. Asterisk: focal source. Solid arrows: stable rotors. Dotted arrows: spurious rotors.

4.2. Optical map recordings

Fig. 2.1A shows a constant left-tight and up-down propagation during sinus rhythm. The RM (Fig. 2.1B) presents the highest value (i.e. 0.0076) in the nearest corner to the stimulation point, whereas other regions of the tissue presented values closer to zero.

Figure 2.2A shows one frame of a phase map of a recording from the LAA. During the recording period two rotors are formed in the left of the field view, forming a figure of eight (Fig. 2.2A). The RM map shows higher values at the position of those two stable rotors (i.e. 0.0054 and 0.0041 respectively). Notice that maximum P values in real experiments are lower than those computed for mathematical simulation since real recordings include noise and drifting rotors instead of stationary rotors. Other regions of the tissue show values as low as those obtained in mathematical simulations.

In Fig. 2.3A, an example where three or more singularity points were detected during the entire recording is depicted. Most rotors appear after the collision of other wavefronts and disappear after few frames. However, one rotor remains stable during the entire recording and maybe considered as the mother rotor of the entire fibrillatory activity. The RM shows an area with higher value (i.e. 0.0048), corresponding with the position of that stable rotor. For this disorganized fibrillation process, the RM show areas with gray values indicating that during some interval periods those regions were governed by their surrounding tissue.

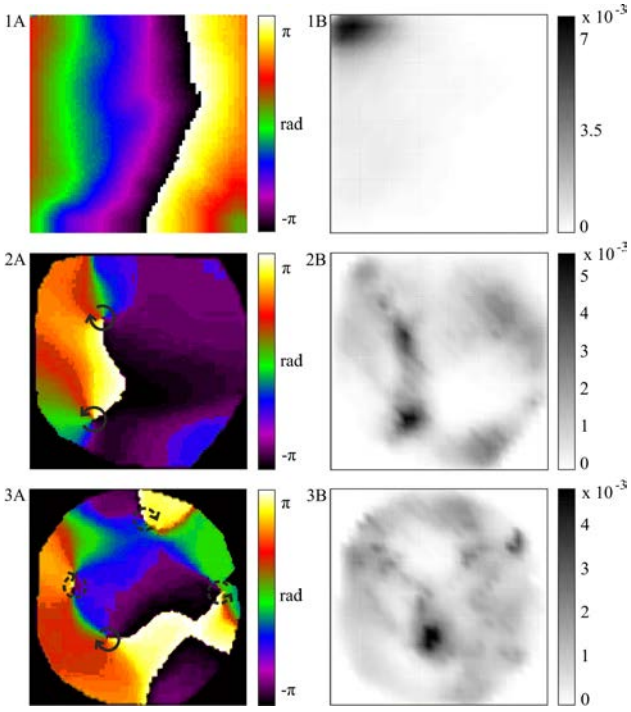

Figure 2. Phase Map (A) and Recurrence Map (B) from the optical mapping recordings: (1) Pacing, (2) LAA, (3) PLA. Solid arrows: stable rotors. Dotted arrows: spurious rotors.

4. Discussion

The present study describes a novel methodology to identify the areas of the myocardium that can be the responsible of the onset and/or maintenance of a fibrillatory process. The applicability of the presented methodology has been described by using mathematical simulations and tested by using optical mapping recordings. Our results demonstrate that, in case that the fibrillatory process is governed by the presence of a single rotor or a focus, the causal relationship allows its identification even in presence of secondary rotors. Additionally, the recurrent map also allows the detection of multiple dominating rotors.

As presented in previous works [4-5], the causality-based analysis is able to identify the propagation pattern which governs the electrical activity in the myocardium. Causality analysis has been used to identify the propagation pattern during AF. However, interpretation of a causal relationship map may be complex. In this study, we summarized causal relations in a single map which indicates which areas of the tissue govern the activity of its surroundings.

Since Haissaguerre et al. demonstrated that the ablation of specific regions of the atrium that are responsible of the maintaining of the fibrillatory process allows the termination of the arrhythmia [3], several approaches have been used in order to identify ablation targets. Atienza et al. [6] used a dominant-frequency guided ablation procedure and demonstrated that the isolation of atrial regions with higher dominant frequency reduced the AF recurrence in patients with frequency gradients. Other authors have focused on the ablation of atrial regions with complex fractionated electrograms (CFAEs) [7]. Causal relations analysis present the advantage over a dominant-frequency approach that foci can be detected in the absence of a frequency gradient and may enable to determine whether high frequency regions are activity sources or wavefront collision regions. As compared to the CFAE approach, causal analysis may allow determining whether a given fractionated electrogram result from microreentry or, instead, result from collision or slow conduction at fibrotic tissue. Analysis of causal relations, therefore, may overcome some of the important limitations of current methods for locating AF sources. Recurrence maps may be useful to characterize AF mechanisms on each individual patient and may be useful as guidance for an ablation procedure.

Acknowledgements

Supported in part by Spanish Ministry of Economy (TEC2009-13939); Universitat Politècnica de València through its research initiative program and Generalitat Valenciana Grants (AP-145/10, PROMETEO/2010/093).

References

[1] Moe G. On the multiple wavelet hypothesis of atrial fibrillation. Arch Int Pharmacodyn Ther 1962;140:183-188.
[2] Jalife J. Déjà vu in the theories of atrial fibrillation dynamics. Cardiovascular Res 2011;89:766-75.
[3] Haïssaguerre M, Jaïs P, Shah DC., et al. Spontaneous initiation of atrial fibrillation by ectopic beats originating in the pulmonary veins. N Engl J Med 1998;339:659-66.
[4] Rodrigo M, Liberos A, Guillem MS, et al. Causality relation map: anovel methodology for the identification of hierarchical fibrillatory processes. Computing in cardiology 2011;38:173-176.
[5] Richter U, Faes L, Cristoforetti A, et al. A novel approach to propagation pattern analysis in intracardiac atrial fibrillation signals. Ann Biomed Eng. 2011;39(1):310-23
[6] Atienza F, Almendral J, Moreno J, et al. Activation of inward rectifier potassium channels accelerates atrial fibrillation in humans: evidence for a re-entrant mechanism. Circulation 2006;114:2434-42.
[7] Di Biase L, Elayi CS, Fahmy TS, et al. Atrial fibrillation ablation strategies for paroxysmal patients: randomized comparison between different techniques. Circ Arrhythm Electrophysiol 2009;2:113-9.

Address for correspondence.
M. Rodrigo
BioITACA, Universitat Politecnia de Valencia,
mirodbor@teleco.upv.es